Optical properties of armchair graphene nanoribbons embedded in hexagonal boron nitride lattices

Hamed Nematian,[1,a)] Mahdi Moradinasab,[2,3] Mahdi Pourfath,[2,3] Morteza Fathipour,[2] and Hans Kosina[3]
[1]*Department of Electrical Engineering, Science and Research Branch, Islamic Azad University, Tehran, Iran*
[2]*School of Electrical and Computer Engineering, University of Tehran, Tehran, Iran*
[3]*Institute for Microelectronics, Technische Universität Wien, Gußhausstraße 27–29/E360, A-1040 Wien, Austria*

(Received 13 March 2012; accepted 28 March 2012; published online 4 May 2012)

Transition rules and optical properties of armchair graphene nanoribbons embedded in hexagonal boron nitride lattices are studied for the first time. Based on tight binding calculations considering first and second nearest neighbors, we show that the optical transition rules of such structures are completely different from that of conventional graphene nanoribbons. These rules are explained by the symmetry properties of the subband wave functions. The optical spectrum, the quantum efficiency, and the photoresponsivity of different nanoribbons are evaluated and their application in photodetector devices is investigated. The results are verified with first principles calculations.
 [http://dx.doi.org/10.1063/1.4710988]

I. INTRODUCTION

Graphene, a single layer carbon sheet with a honeycomb structure, has become a major topic in many areas of research including condensed matter, material physics, chemistry, and device physics. One-dimensional graphene nanoribbons (GNRs) have recently attracted much interest as they are recognized as promising building blocks for nano-electronic devices.[1] Armchair GNRs (AGNRs), a type of GNRs with armchair edges, introduce a tunable bandgap which is suitable for electronic and optical applications.[2]

Recently, single-layer hexagonal boron nitride (h-BN), which is a wide-bandgap semiconductor,[3] and boron nitride nanoribbons (BNNRs) have been studied.[3,4] BNNRs are expected to be produced using a single-layer h-BN as the starting material.[3] The properties of BNNRs are qualitatively different from that of hydrogen-passivated AGNRs (H-AGNRs) because of the relatively large ionicities of B and N atoms and the larger energy-gaps of h-BN.[3] Carbon atoms incorporated in a BN lattice have a stable hexagonal configuration and can form a one-dimensional nanoribbon under suitable chemical potential conditions.[4] It has been shown that AGNRs embedded in BN sheets (AGNRs/BN) are semiconductors.[4] In Ref. 5, the electronic band-structure of AGNRs/BN is investigated. It is shown that AGNRs/BN exhibit a larger bandgap compared to H-AGNRs. The bandgap opening in these structures is primarily due to the perturbation of the on-site potentials of the edge atoms.[5] A relatively large bandgap of AGNRs/BN renders them as suitable candidates for opto-electronic applications. Structures composed of GNRs and BNNRs introduce more flexibility for electronic and opto-electronic applications. In this work, we report for the first time a theoretical study of the optical properties of AGNRs/BN.

The paper is organized as follows. Tight binding model and first principle simulation parameters employed in this study are presented in Sec. II. In Sec. III, the transition rules, dielectric function, quantum efficiency, and photoresponsivity of AGNRs/BN are discussed. Finally, Sec. IV provides concluding remarks.

II. METHODOLOGY

The electronic transport and optical properties of graphene based structures are mostly determined by the π orbitals.[6] A first nearest neighbor tight-binding (TB) approximation has been widely used to model the electronic properties of such structures.[7,8] To study AGNR/BN, however, a TB model incorporating at least two nearest neighbors is required.[5] Reference 5 has shown that the band structure of AGNRs/BN can be calculated within the desired precision assuming the orthogonality of atomic orbitals and considering the effect of more nearest neighbors for each atom. Therefore, the Hamiltonian can be written as[5]

$$H = \sum_i \varepsilon_i (c_i c_i^{\dagger}) + \sum_{i,j} t_{ij} (c_i c_j^{\dagger} + c_j c_i^{\dagger}), \tag{1}$$

where the operator $c_i(c_i^{\dagger})$ creates (annihilates) an electron at some site i and the indices i and j run over all of the atoms in the unit cell, ε_i is the on-site energy for i-th atom, and t_{ij} is the hopping parameter between i-th and j-th atoms. Reference 9 shows that taking the effect of the first three neighboring atoms into consideration results in a good agreement with first principle calculations. Also, considering the second nearest neighbor carbon atoms in TB calculations shifts the dispersion relation by a constant value,[9] thereby affecting the optical transition rules. Therefore, up to second nearest neighbors are included in our work employing the parameters reported in Ref. 5.

To investigate the optical response of AGNRs/BN, the incident light is assumed to be polarized along the transport direction (x-axis). Particularly, it is shown that the photocurrent is maximized for photons polarized along the longitudinal

a)Electronic mail: h.nematian@ieee.org.

direction of the structure,[10] which are the main source for interband transitions.[11–13]

We compare our TB results with first principles calculations employing SIESTA[14] with the following parameters: double-ζ basis set with additional orbitals of polarization for total energies and electronic band-structures calculations, the generalized gradient approximation method, Perdew-Burke-Ernzerhof (PBE) as the exchange-correlation function, and the Troullier-Martins scheme for the norm-conserving pseudopotential calculations.[5] A grid cutoff of 210 Ry is used and the Brillouin zone sampling is performed by the Monkhost pack mesh of k-points. A mesh of $(128 \times 8 \times 1)$ has been adopted for discretization of k-points and a broadening factor of 0.1eV is assumed for the joint density of states (JDOS) calculation. The optical polarization vector is assumed to be along the transport direction similar to the assumption made in the TB calculation.

III. RESULTS AND DISCUSSIONS

A. Transition rules

The interband optical matrix element for a transition from an eigenstate in the valance subband $|\psi_v\rangle$ to another eigenstate in the conduction subband $|\psi_c\rangle$ is given by $(e/m_0)\langle\psi_c|\mathbf{A}\cdot\mathbf{p}|\psi_v\rangle$,[15] where e is the elementary charge, m_0 is the electron mass, $\mathbf{A} = A\hat{\mathbf{e}}$ is the vector potential, $\hat{\mathbf{e}}$ is a unit vector parallel to $\mathbf{A}$, and $\mathbf{p}$ is the linear momentum operator. The vector potential can be taken out of the expectation value assuming dipole approximation.[15] As a result, by evaluating momentum matrix elements, $\langle\psi_c|\hat{\mathbf{e}}\cdot\mathbf{p}|\psi_v\rangle$, optical transition rates can be achieved. Since the electromagnetic field is assumed to be parallel along the x direction, therefore

$$p_{n,m} = \langle\psi_c|p_x|\psi_v\rangle. \tag{2}$$

These matrix elements determine the selection rules for optical transitions.[16] A zero matrix element means a forbidden transition. To determine a transition rule, it is sufficient to determine the symmetry of the transition matrix element. If the symmetry of this element spans the totally symmetric representation of the point group to which the unit cell belongs then its value is not zero and the transition is allowed. Otherwise, the transition is forbidden. Assuming a uniform potential profile across the ribbon's width, the subband's wave functions are either symmetric or anti-symmetric along the y-axis direction ($\langle -y|\psi_{c/v}\rangle = \pm\langle y|\psi_{c/v}\rangle$). Therefore, the momentum matrix elements are non-zero for interband-transitions from the symmetric (anti-symmetric) to the symmetric (anti-symmetric) wave functions. This transition rule results in transitions from subbands with odd (even) to odd (even) indices in AGNRs/BN, which is described later.

Figure 1 shows the structure of an AGNR/BN which is represented by AGNRn_{cc} BNm_{bn}, where n_{cc} is the number of carbon dimers in the unit cell of the AGNR and $m_{bn} = m_{bnu} + m_{bnl}$ is the summation of the upper and lower BNNRs dimers.

The wave functions at the sublattices A and B of an $AGNR_{20}BN_{40}$ at $k_x = 0$ are shown in Fig. 2. $C_{A/B}$, $N_{A/B}$, and $B_{A/B}$ represent the components of the wave functions at

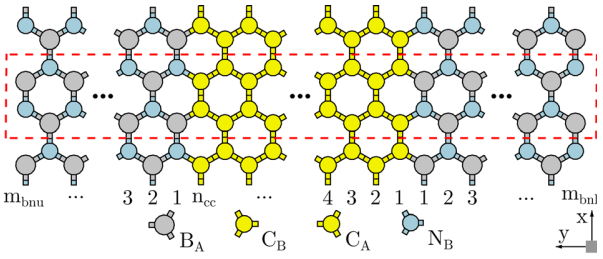

FIG. 1. The structure of an AGNRn_{cc} BNm_{bn}. The incident light is assumed to be polarized along the x-direction. $C_{A/B}$, $N_{A/B}$, and $B_{A/B}$ represent a carbon, a nitrogen, and a boron atom at the sublattice A or B.

carbon, nitrogen, and boron atoms at some sublattice A or B. The wave function of each subband is the summation of the wave functions at these two sublattices. For example, the wave functions for the subband indices $n_v = 60$ (Figs. 2(g) and 2(h)), $n_c = 2$ (Figs. 2(i) and 2(j)), and $n_c = 60$ (Figs. 2(a) and 2(b)) are anti-symmetric. Therefore, as discussed before, the matrix elements are non-zero for transitions from $n_v = 60$ to $n_c = 2$ and $n_c = 60$. The transitions from $n_v = 59$ to $n_c = 1$ and $n_c = 59$ are also possible as their respective wave functions are symmetric. With the same analysis, a transition from the highest valence subband to the lowest conduction subband ($n_v = 1$ to $n_c = 1$) is possible in AGNRs/BN (see Figs. 2(m), 2(n), 2(k), and 2(l)).

One can approximate the wave functions of an H-AGNR at pth atomic site with $\sin(n\theta p)$ functions, where n is the subband index and $\theta = \pi/(N+1)$ (see Appendix A). Considering such wave functions, one can calculate the momentum matrix elements using

$$p_{n,m}(k_x) = \frac{1}{(N+1)}\frac{im_0}{\hbar}ta_{cc}\left[\sum_{p=1}^{N}\sin(n\theta p)\sin(m\theta p)\right]F_{n,m}(k_x). \tag{3}$$

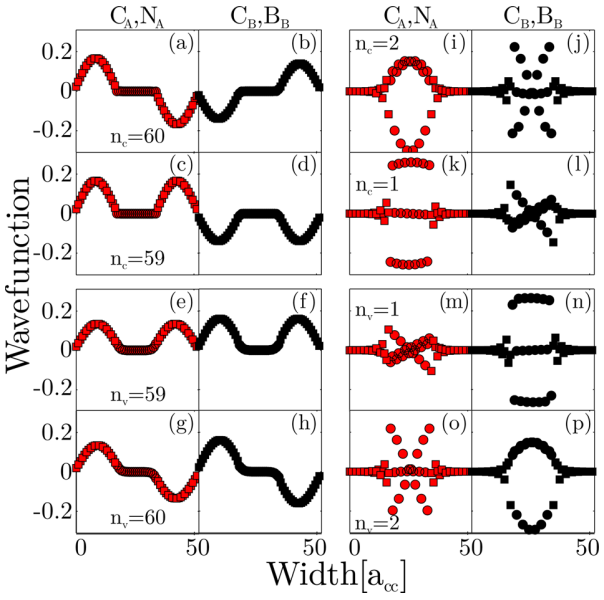

FIG. 2. The wave functions of a $AGNR_{20}BN_{40}$ at C_A (red circles), N_A (red squares), C_B (black circles), and B_B (black squares). $n_c = 1$ ($n_v = 1$) represents the lowest conduction (highest valence) subband.

According to this equation, only transitions between valence and conduction subbands with the same band-index are allowed (shown in Appendix B). As shown in Fig. 2, the wave functions for AGNRs/BN are not necessarily a single sinusoidal function. The Fourier series of these wave functions contain sinusoidal functions with different arguments and coefficients, which results in more allowed interband-transitions compared to H-AGNRs. Non-zero terms and the symmetry properties of the AGNR/BN wave functions indicate that the interband-transitions between subbands with the same parity are allowed (odd to odd and even to even). This transition rule is more restricted for conventional H-AGNRs where the wave functions consist of complete sine terms (see Eq. (B6).[17] The rules are also different from that of ZGNRs where interband-transitions from subbands with odd (even) indices to subbands with even (odd) indices are allowed.[18]

B. Dielectric function

In the linear response regime, the imaginary part of the dielectric function is given by[15]

$$\varepsilon_i(\omega) = \frac{1}{4\pi\varepsilon_0}\left(\frac{2\pi e}{m\omega}\right)^2 \sum_{\mathbf{k_x}} |p_{c,v}|^2 \delta\left(E_c(\mathbf{k_x}) - E_v(\mathbf{k_x}) - \hbar\omega\right) \times \left[f\left(E_v(\mathbf{k_x})\right) - f\left(E_c(\mathbf{k_x})\right)\right], \quad (4)$$

where $\hbar\omega$ is the energy of the incident photons. The Dirac delta is approximated by a Gaussian function with a broadening factor of 0.1 eV.

The summation in Eq. (4) can be converted into a energy integration by introducing the JDOS defined as

$$D_j(\hbar\omega) = \frac{1}{\pi}\int_{S_{k_x}} \frac{dS}{\left|\nabla_{k_x}\left(E_c(\mathbf{k_x}) - E_v(\mathbf{k_x})\right)\right|}, \quad (5)$$

where S_{k_x} is the constant energy surface defined by $E_c(\mathbf{k_x}) - E_v(\mathbf{k_x}) = \hbar\omega$.

The real part of the dielectric function $\varepsilon_r(\omega)$ can be evaluated from the imaginary part using the Kramers-Kronig relation.[15] The interband dielectric function is related to the optical conductivity by $\varepsilon(\omega) = 1 + 4\pi i\sigma(\omega)/\omega$.[11] In Fig. 3(a), $\varepsilon_i(\omega)$ and the JDOS of $AGNR_{20}BN_{40}$ are plotted. In the energy range. $0 < \hbar\omega < 2$eV, the JDOS has maxima at $\hbar\omega = 0.3019, 0.62214, 0.92657, 0.91883, 1.2289, 1.5256$, and 1.7349eV. However, only four of these maxima ($\hbar\omega = 0.3019, 0.91883, 0.92657$, and 1.5256eV) appear in $\varepsilon_i(\omega)$. From the electronic band-structure in Fig. 3(b), it can be shown that the peaks in $\varepsilon_i(\omega)$ are related to transitions from $n_v = 1$ to $n_c = 1$ (A), $n_v = 1$ to $n_c = 3$ (B), $n_v = 2$ to $n_c = 2$ (C), and $n_v = 2$ to $n_c = 4$ (D). Disappeared peaks in $\varepsilon_i(\omega)$ are due to zero momentum matrix elements in Eq. (4). This transition rule confirms previous results which are explained by the symmetry properties of the wave functions.

Figure 3(a) compares the dielectric functions of an $AGNR_{20}BN_{40}$ obtained from TB and first principle calculations. Excellent agreement between these results confirms the transition rules obtained from TB calculations. The energy of the first peak matches well, however, the discrepancies

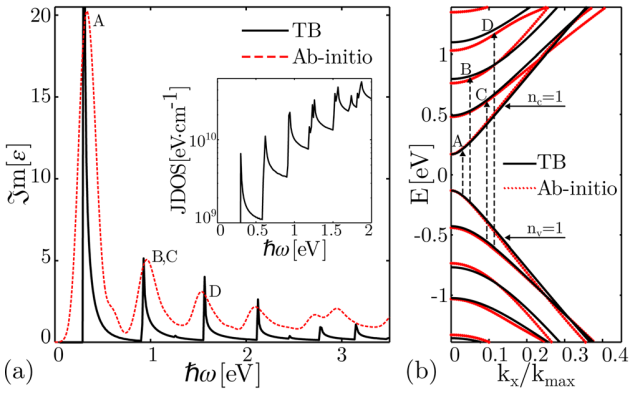

FIG. 3. (a) The dielectric function of an $AGNR_{20}BN_{40}$ based on TB (solid line) and first principle calculations (dashed line). The inset shows the related JDOS using the TB model. (b) The electronic band-structure of an $AGNR_{20}BN_{40}$ from TB (solid line) and first principle calculations (red dotted line).

increase for higher peaks. This behavior is related to the differences between the predicted energy-gaps obtained from SIESTA and TB at higher energies, see Fig. 3(b).

C. Quantum efficiency

In order to investigate AGNRs/BN for photodetection application, we study the quantum efficiency defined as $\alpha = (I_{ph}/q)/(P_{op}/\hbar\omega)$, where I_{ph} is the photo current and P_{op} is the incident optical power. We assumed that all absorbed photons contribute to the photo current, such that the quantum efficiency can be calculated from the dielectric function (Eq. (4)). A quantum efficiency of $6-16\%$ for graphene is reported in Ref. 19 and a maximum quantum efficiency ranging from 9% to 11% is reported for H-AGNRs in Ref. 20. Figure 4 shows the calculated quantum efficiency as a function of the incident photon energy at various GNR widths. The efficiency is maximized when the photon energy matches the bandgap of the nanoribbon (the first peak for each structure). Our results indicate a peak of quantum efficiency in the range of $14-15\%$ for AGNRs/BN. The quantum efficiencies of photodetectors based on AGNRs/BN and H-AGNRs are compared in Fig. 4. Due to the presence of more allowed transitions, a wider absorption spectrum is achieved in AGNRs/BN compared to H-AGNRs. As a H-AGNR with index 8 is metallic, the first peak is related to the second energy-gap and appears at 2.88eV whereas the $AGNR_8BN_{30}$ shows three peaks below that energy due to energy-gap opening, see Fig. 4(a). In Fig. 4, the quantum efficiency decreases for the first energies, but increases at higher energies, see for example, the sixth peak for $AGNR_{33}BN_{30}$. This is due to different effective masses of different subbands which affect the JDOS. According to Eq. (4), a larger JDOS leads to a larger absorption of photons and a higher quantum efficiency.

We also investigate the photoresponsivity given by (I_{ph}/P_{op}). Our calculations give an upper limit for the photoresponsivities of 0.336 A/W, 0.239 A/W, and 0.202 A/W for photon energies near the bandgaps of $AGNR_8BN_{30}$, $AGNR_{16}BN_{30}$, and $AGNR_{33}BN_{30}$, respectively. Due to the higher quantum efficiency of AGNRs/BN compared to AGNRs, a higher photoresponsivity is obtained for the same input optical power of 10^7 W/m^2.

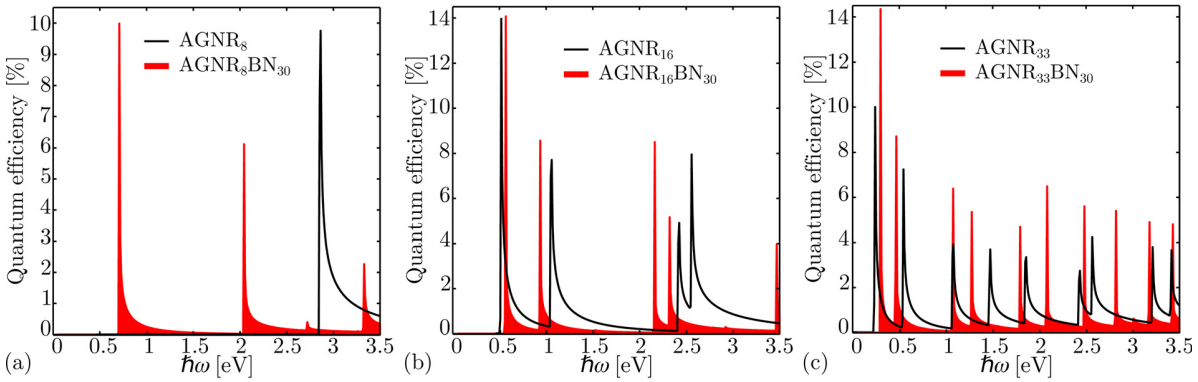

FIG. 4. The quantum efficiency of an (a) $AGNR_8BN_{30}$, (b) $AGNR_{16}BN_{30}$, and (c) $AGNR_{33}BN_{30}$ compared to a H-AGNRs with the same indices.

IV. CONCLUSIONS

In summary, we theoretically studied the optical properties of AGNRs/BN, employing TB calculations. We demonstrate that in AGNRs/BN only optical transitions from subbands with odd (even) indices to subbands with odd (even) indices are allowed. This transition rule is more restricted for AGNRs and completely different from that of ZGNRs. Our TB results are in agreement with first principle calculations which verify the accuracy of our model. The applicability of AGNRs/BN as photodetectors is investigated. Our results indicate that due to more allowed transitions compared to conventional GNRs a larger photo current in AGNR/BN structures can be achieved. The results render AGNRs/BN as suitable candidates for infrared photodetectors and future optoelectronic applications.

APPENDIX A: SUBBAND WAVE FUNCTIONS

The total wave function of the system is given by[21]

$$|\psi\rangle = C_A|\psi_A\rangle + C_B|\psi_B\rangle. \tag{A1}$$

The Bloch wave functions $|\psi_A\rangle$ and $|\psi_B\rangle$ can be expressed as a linear combination of atomic wave functions of $2p_z$ orbitals $|A_p\rangle$ and $|B_q\rangle$. Due to translational invariance along the x direction, one obtains

$$\begin{aligned} |\psi_A\rangle &= \frac{1}{\sqrt{\Omega_A}}\sum_{p=1}^{N} e^{ik_x x_p^A}\phi_p|A_p\rangle, \\ |\psi_B\rangle &= \frac{1}{\sqrt{\Omega_B}}\sum_{p=1}^{N} e^{ik_x x_p^B}\phi_p|B_p\rangle, \end{aligned} \tag{A2}$$

where $\Omega_{A/B}$ are the normalization factors, N is the number of A and B sublattices in the unit-cell of the GNR, $x_p^{A/B}$ are the x-positions of the pth A/B-type carbon atom, ϕ_p is the y direction component of the wave functions at the p th lattice site. We impose hard-wall boundary conditions[22] at the edges, $\phi_0 = 0$ and $\phi_{N+1} = 0$. Therefore, one can assume that the component of the wave functions in the y direction form standing waves,

$$\phi_p = \sin\left(\frac{\pi n}{N+1}p\right) = \sin(n\theta p), \qquad n = 1, 2, \ldots, N, \tag{A3}$$

where n is the band index. For convenience, the notation $\theta = \pi/(N+1)$ is introduced. Assuming the normalization condition $\langle\psi_A|\psi_A\rangle = \langle\psi_B|\psi_B\rangle = 1$,[22] the prefactors are obtained as $\Omega_A = \Omega_B = N_x(N+1)/2$, where N_x is the number of unit cells along the x direction. For a perfect and uniform ribbon we just need to perform the calculations over one unit-cell, therefore, from here on we assume $N_x = 1$. Finally, the coefficients C_A and C_B in Eq. (1) are found by solving the Schrödinger equation, $H|\psi\rangle = E|\psi\rangle$, resulting in $C_B = \pm C_A e^{-i\varphi_n(k_x)}$, where $\varphi_n(k_x)$ is defined as

$$e^{i\varphi_n(k_x)} = \frac{f_n(k_x)}{|f_n(kx)|}, \tag{A4}$$

in which $f_n(k_x) = e^{ik_x a_{cc}} + 2e^{-ik_x a_{cc}/2}\cos(n\theta)$. To satisfy the normalization condition, $|C_A|^2 + |C_B|^2 = 1$, one can choose $C_A = 1/\sqrt{2}$ and $C_B = \pm e^{-\varphi_n(k_x)}/\sqrt{2}$. The wave function is given by

$$\begin{aligned} |\pm, n, k_x\rangle = \frac{1}{\sqrt{(N+1)}}\Bigg[\sum_{p=1}^{N}\Big(&e^{ik_x x_p^A}\sin(n\theta p)|A_p\rangle \\ &\mp e^{-i\varphi_n(k_x)}e^{ik_x x_p^B}\sin(n\theta p)|B_p\rangle\Big)\Bigg], \end{aligned} \tag{A5}$$

where the notation $|\pm, n, k_x\rangle \equiv |\psi_n^{\pm}(k_x)\rangle$ is introduced and $\pm$ denote the conduction and the valence bands, respectively.

APPENDIX B: OPTICAL TRANSITION RULES

To obtain the momentum matrix elements $(p_{c,v})$ in Eq. (4), the gradient approximation is employed. By using the operator relation $\mathbf{p} = (im_0/\hbar)[H, \mathbf{r}]$, Eq. (2) can be written as $p_{c,v} = (im_0/\hbar)\langle c|Hx - xH|v\rangle$. By neglecting intra-atomic transitions the momentum matrix elements can be approximated as[23]

$$p_{c,v} = (x_v - x_c)\frac{im_0}{\hbar}\langle c|H|v\rangle. \tag{B1}$$

Using this approximation and the wave function Eq. (A5) momentum matrix elements are obtained as

$$p_{n,m}(k_x) = \frac{1}{(N+1)}\frac{im_0}{\hbar}\sum_{p=1}^{N}\sum_{q=1}^{N}\Big[+ (x_q^B - x_p^A)e^{ik_x(x_q^B - x_p^A)}\sin(n\theta p)\sin(m\theta q)\langle A_p|H|B_q\rangle e^{-i\varphi_m(k_x)} - (x_q^A - x_p^B)e^{ik_x(x_q^A - x_p^B)}\sin(n\theta p)\sin(m\theta q)\langle B_p|H|A_q\rangle e^{+i\varphi_n(k_x)}\Big], \tag{B2}$$

where $\langle A_p|H|B_q\rangle = \langle B_p|H|A_q\rangle = t$ for $p = q$ and $p = q \pm 1$, otherwise the matrix elements are zero. Therefore, Eq. (B2) can be written as

$$\begin{aligned} p_{n,m}(k_x) &= \frac{1}{(N+1)}\frac{im_0}{\hbar}ta_{cc}\sum_{p=1}^{N}\sin(n\theta p)\Big[+ e^{-i\varphi_m(k_x)} + \Big(e^{+ik_x a_{cc}}\sin(m\theta p) - \frac{1}{2}e^{-ik_x a_{cc}/2}\Big[\sin\Big(m\theta(p-1)\Big) + \sin\Big(m\theta(p+1)\Big)\Big]\Big) \\ &\quad - e^{+i\varphi_n(k_x)}\Big(-e^{-ik_x a_{cc}}\sin(m\theta p) + \frac{1}{2}e^{+ik_x a_{cc}/2}\Big[\sin\Big(m\theta(p-1)\Big) + \sin\Big(m\theta(p+1)\Big)\Big]\Big)\Big]. \\ &= \frac{1}{(N+1)}\frac{im_0}{\hbar}ta_{cc}\Big[\sum_{p=1}^{N}\sin(n\theta p)\sin(m\theta p)\Big] \times \Big(+ e^{-i\varphi_m(k_x)}\Big(e^{+ik_x a_{cc}} - e^{-ik_x a_{cc}/2}\cos(m\theta)\Big) \\ &\quad + e^{+i\varphi_n(k_x)}\Big(e^{-ik_x a_{cc}} - e^{+ik_x a_{cc}/2}\cos(m\theta)\Big)\Big). \end{aligned} \tag{B3}$$

Here, the relation $\sin(x) + \sin(y) = 2\sin\Big((x+y)/2\Big)\cos\Big((x-y)/2\Big)$ is employed. Using Eq. (A4), Eq. (B3) can be written as

$$\begin{aligned} p_{n,m}(k_x) &= \frac{1}{(N+1)}\frac{im_0}{\hbar}ta_{cc}\Big[\sum_{p=1}^{N}\sin(n\theta p)\sin(m\theta p)\Big] \\ &\quad \times \underbrace{\Big(+ \frac{1}{|f_m(k_x)|}\Big(1 - 2\cos^2(m\theta) + 2e^{+i3k_x a_{cc}/2}\cos(m\theta) - e^{-i3k_x a_{cc}/2}\cos(m\theta)\Big) + \frac{1}{|f_n(k_x)|}\Big(1 - 2\cos(m\theta)\sin(n\theta) + 2e^{-i3k_x a_{cc}/2}\cos(n\theta) - e^{+i3k_x a_{cc}/2}\cos(m\theta)\Big)\Big)}_{F_{n,m}(kx)}. \\ &= \frac{1}{(N+1)}\frac{im_0}{\hbar}ta_{cc}\Big[\sum_{p=1}^{N}\sin(n\theta p)\sin(m\theta p)\Big]F_{n,m}(k_x). \end{aligned} \tag{B4}$$

The summation over sine functions in Eq. (B4) determines the transition rules. Using some trigonometric identities one can write this summation as

$$\begin{aligned} \sum_{p=1}^{N}\sin(n\theta p)\sin(m\theta p) &= \frac{1}{2}\Big[+ \cos\frac{(n-m)\pi}{2}\sin\frac{(n-m)\pi N}{2(N+1)} \\ &\quad \times\Big(\sin\frac{(n-m)\pi}{2(N+1)}\Big)^{-1} - \cos\frac{(n+m)\pi}{2} \\ &\quad \times \sin\frac{(n+m)\pi N}{2(N+1)}\Big(\sin\frac{(n+m)\pi}{2(N+1)}\Big)^{-1}\Big]. \end{aligned} \tag{B5}$$

If $n \pm m = 2k + 1$, where k is a non-zero integer, both terms in the bracket of Eq. (5) will be zero. In the case of $n \pm m = 2k$, both terms in the bracket will be equal to -1, therefore, the summation will be again zero. However, if $n = m$, the fist term in will be equal to N and the second term will be equal to -1. Therefore, only transitions between valence and conduction subbands with the same band-index are allowed

$$\sum_{p=1}^{N}\sin(n\theta p)\sin(m\theta p) = \begin{cases} \dfrac{N+1}{2}, & n = m \\ 0, & n \neq m \end{cases}. \tag{B6}$$

[1]M. Freitag, Nat. Nanotechnol. **3**, 455 (2008).
[2]F. Bonaccorso, Z. Sun, T. Hasan, and A. Ferrari, Nat. Photonics **4**, 611 (2010).
[3]F. Zheng, K.-I. Sasaki, R. Saito, W. Duan, and B.-L. Gu, J. Phys. Soc. Jpn. **78**, 074713 (2009).
[4]Y. Ding, Y. Wang, and J. Ni, Appl. Phys. Lett. **95**, 123105 (2009).
[5]G. Seol and J. Guo, Appl. Phys. Lett. **98**, 143107 (2011).
[6]R. Saito, G. Dresselhaus, and M. Dresselhaus, *Physical Properties of Carbon Nanotubes* (Imperial College Press, London, 1998).
[7]S. Reich, J. Maultzsch, C. Thomsen, and P. Ordejón, Phys. Rev. B **66**, 035412 (2002).
[8]Y. Hancock, A. Uppstu, K. Saloriutta, A. Harju, and M. J. Puska, Phys. Rev. B **81**, 245402 (2010).
[9]D. Gunlycke and C. T. White, Phys. Rev. B **77**, 115116 (2008).
[10]M. Freitag, Y. Martin, J. Misewich, R. Martel, and P. Avouris, Nano Lett. **3**, 1067 (2003).

[11]H. Hsu and L. E. Reichl, Phys. Rev. B **76**, 045418 (2007).
[12]S. Tasaki, K. Maekawa, and T. Yamabe, Phys. Rev. B **57**, 9301 (1998).
[13]A. Grüneis, R. Saito, G. G. Samsomidze, T. Kimura, M. A. Pimenta, A. Jorio, A. G. S. Filho, G. D. Dresselhaus, and M. S. Dresselhaus, Phys. Rev. B **67**, 165402 (2003).
[14]J. M. Soler, E. Artacho, J. D. Gale, A. García, J. Junquera1, P. Ordejón, and D. Sánchez-Portal, J. Phys.: Condens. Matter **14**, 2745 (2002).
[15]P. T. Yu and M. Cardona, *Fundamentals of Semiconductors: Physics and Materials Properties* (Springer, Berlin, 2001).
[16]*Symmetry and Spectroscopy: Introduction to Vibrational and Electronic Spectroscopy*, edited by D. C. Harris and M. D. Bertolucci (Courier Dover Publications, 1989).
[17]K. I. Sasaki, K. Kato, Y. Tokura, K. Oguri, and T. Sogawa, Phys. Rev. B **84**, 085458 (2011).
[18]H. C. Chung, M. H. Lee, C. P. Chang, and M. F. Lin, Opt. Express **19**, 23351 (2011).
[19]F. Xia, T. Mueller, Y.-M. Lin, A. Valdes-Garcia, and P. Avouris, Nat. Nanotechnol. **4**, 839 (2009).
[20]M. Pourfath, O. Baumgartner, S. Kosina, and S. Selberherr, in *Proceedings of the 9th International Conference on Numerical Simulation of Optoelectronic Devices, NUSOD* (IEEE, 2009), p. 13.
[21]S. V. Goupalov, Phys. Rev. B **72**, 195403 (2005).
[22]H. Zheng, Z. Wang, T. Luo, Q. Shi, and J. Chen, Phys. Rev. B **75**, 165414 (2007).
[23]T. G. Pedersen, Phys. Rev. B **67**, 113106 (2003).